

RESEARCH ARTICLE SUMMARY

DNA NANOTECHNOLOGY

Self-assembly of genetically encoded DNA-protein hybrid nanoscale shapes

Florian Praetorius and Hendrik Dietz*

INTRODUCTION: Controlling the spatial arrangement of functional components in biological systems on the scale of higher-order macromolecular assemblies is an important goal in synthetic biology. Achieving this goal could yield new research tools and pave the way for interesting applications in health and biotechnology. DNA origami enables constructing arbitrary shapes on the desired scale by folding a single-stranded DNA “scaffold” into user-defined shapes using a set of “staple” oligonucleotides, but single-stranded DNA is typically not available in living cells, and the structures usually assemble only at nonphysiological temperatures. The scope of functions that can be fulfilled by DNA itself appears so far still limited. Proteins, on the other hand, offer a large variety of functionalities and are easily accessible in cells through genetic encoding, but designing larger structural frameworks from proteins alone remains challenging.

RATIONALE: Here, we reimagined DNA origami to explore the possibility for using a set of designed proteins to fold a double-stranded DNA template into user-defined DNA-protein hybrid objects with dimensions on the desired

10- to 100-nm scale. To realize our idea, we require synthetic DNA “looping” proteins that can link two user-defined double-helical DNA sequences, and we need to determine suitable rules for arranging both the template and multiple of such staple proteins in the context of a larger target structure. Transcription activator-like (TAL) effector proteins are produced by plant pathogenic bacteria and injected into host cells, where they bind to specific promoter regions, thus controlling the expression of target genes. The DNA recognizing part of a TAL effector consists of an array of repeat subunits that binds to the major groove of double-helical DNA, thus forming a superhelix. Each repeat subunit comprises ~34 amino acids and recognizes a single DNA base pair. Because of their modular architecture, TAL effectors can be engineered to bind to user-defined DNA sequences, and this technique is currently being exploited for genome engineering applications. For constructing the staple proteins, we therefore chose the DNA-recognizing domains of TAL effectors.

RESULTS: We characterized the DNA-recognizing domains of the TAL effectors with respect to

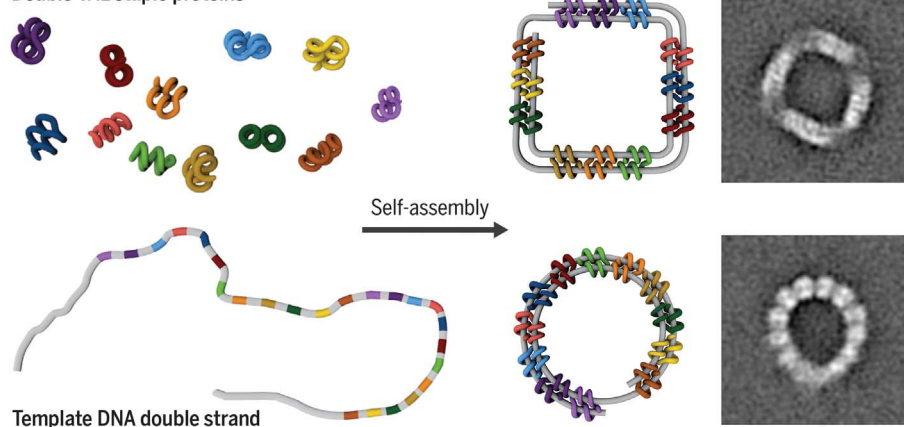
binding affinity and sequence specificity. To construct the staple proteins, we fused two TAL proteins via a custom peptide linker and tested for the ability to connect two separate double-helical DNA domains. For creating larger objects containing multiple staple protein connections, we identified a set of rules regarding the optimal spacing between these connections. On the basis of these rules, we could create megadalton-scale objects that realize a variety of structural motifs, such as custom curvatures, vertices, and corners. Each of those objects was built from a set of 12 double-TAL staple proteins and a template DNA double strand with designed sequence. We also tested design principles for multilayer structures with enhanced rigidity. All components of our nanostructures can be genetically encoded and self-assemble isothermally at room temperature in near-physiological buffer conditions. The staple proteins used in this work also carried a green fluorescent protein domain that serves as a placeholder for a variety of functional protein domains that can be genetically fused to the staple proteins. We were also able to demonstrate formation of our structures starting from genetic expression in a one-pot reaction mixture that contained the double-stranded DNA scaffold, the genes encoding the staple proteins, RNA polymerase, ribosomes, and cofactors for transcription and translation. Successful self-assembly of our hybrid nanostructures was confirmed using transmission electron microscopy.

ON OUR WEBSITE

Read the full article at <http://dx.doi.org/10.1126/science.aam5488>

CONCLUSION: By using our system of designing double-TAL staple proteins that fold a template DNA double strand, researchers can control the spatial arrangement of protein domains in custom geometries. Our system should have a good chance to work inside cells, given the success of our *in vitro* expression experiments and considering that the DNA binding properties of TAL are preserved inside cells, as seen in gene editing experiments with TAL-based endonucleases. Because TAL-based staple proteins can be tailored to specifically recognize any desired DNA target sequence, these proteins could then be used to create custom structures and loops in genomic DNA to study the relation between genome architecture and gene expression, or to position proteins involved in other intracellular processes in user-defined ways. ■

Double-TAL staple proteins



Schematic illustration of the self-assembly of DNA-protein hybrid objects from a set of 12 double-TAL staple proteins and a template DNA double strand. Depending on the sequence of the template, the resulting object may be a square (**top**) or a double-ring circle (**bottom**). In total, we designed 18 different protein hybrid objects using this principle. Scale bar, 20 nm.

Physics Department and Institute for Advanced Study, Technische Universität München, Garching bei München, Germany.

*Corresponding author. Email: dietz@tum.de

Cite this article as F. Praetorius, H. Dietz, *Science* 355, eaam5488 (2017). DOI: 10.1126/science.aam5488

RESEARCH ARTICLE

DNA NANOTECHNOLOGY

Self-assembly of genetically encoded DNA-protein hybrid nanoscale shapes

Florian Praetorius and Hendrik Dietz*

We describe an approach to bottom-up fabrication that allows integration of the functional diversity of proteins into designed three-dimensional structural frameworks. A set of custom staple proteins based on transcription activator–like effector proteins folds a double-stranded DNA template into a user-defined shape. Each staple protein is designed to recognize and closely link two distinct double-helical DNA sequences at separate positions on the template. We present design rules for constructing megadalton-scale DNA-protein hybrid shapes; introduce various structural motifs, such as custom curvature, corners, and vertices; and describe principles for creating multilayer DNA-protein objects with enhanced rigidity. We demonstrate self-assembly of our hybrid nanostructures in one-pot mixtures that include the genetic information for the designed proteins, the template DNA, RNA polymerase, ribosomes, and cofactors for transcription and translation.

Designing genetically encoded scaffold structures for the controlled spatial arrangement of multiple functionalities on the 10- to 100-nm scale is an important unmet challenge for synthetic biology and biotechnology. Such objects would be of interest for fundamental research, medicine, and industrial biotechnology. For example, controlling the spatial arrangement of molecules in cells could help researchers to explore the connection between spatial order and function on multiple scales, in particular in the context of gene regulation (1) and in signaling (2, 3). Therapeutically active assemblies could be envisioned whose function is logically connected to cellular processes. Scaffolding of multiple enzymes into a common three-dimensional (3D) framework could also facilitate the production of desired compounds more efficiently in engineered cells or cell extracts (4).

Natural and designed proteins provide access to a vast library of functional modules for molecular recognition and enzymatic catalysis (5–8), and proteins can also serve as hubs for forming higher-order assemblies (9, 10). DNA nanotechnology (11), on the other hand, offers the possibility to construct arbitrary shapes (12–17), periodic arrays (18–21), and mechanisms (22–24) with overall or repeat unit dimensions ranging from tens to hundreds of nanometers. Integrating protein-based functionalities into designed DNA-based structural scaffolds could thus provide an attractive approach toward creating multifunctional assemblies with user-defined shapes (25–28). However, although proteins can easily be genetically encoded and produced in vivo, the encoding and assembly of complex DNA-based structures inside cells face major hurdles. For example, DNA

nanostructures typically cannot fold without prior annealing at elevated temperatures (29), and such objects assemble from DNA single strands, which are not easily available inside living cells. Designed RNA-based nanostructures could potentially be assembled inside cells through cotranscriptional folding (30); however, it is not yet clear how additional functionalities could be integrated into such RNA scaffolds.

Design of staple proteins

We reimagined the scaffolded DNA origami design principle (12) from DNA nanotechnology. In contrast to DNA origami, which uses DNA single strands as building blocks, our approach uses double-helical DNA and proteins. In our method, a continuous double-helical DNA template with user-defined length assumes the role of a scaffold that is folded into a user-defined 3D arrangement by a set of designed staple proteins (Fig. 1A; see also fig. S1) (31). Each staple protein is tailored to specifically recognize two different double-helical DNA sequences with user-defined separation on the double-helical DNA template. The staple proteins can carry additional functionalities. Inspired by the antiparallel junctions that are often used within DNA nanotechnology (32), we envisioned the use of the staple proteins such that they form an antiparallel crossing when connecting two parallel DNA double helices (Fig. 1).

To construct the staple proteins, we relied on the recognition capabilities for double-helical DNA by transcription activator–like (TAL) effector proteins (33–36). Because of their repetitive structure, TAL effectors offer a programmability that enables the construction of numerous staple proteins targeting any desired DNA sequence. Each DNA-recognizing part within a staple protein consists of an N-terminal domain that comprises 100 amino acids, together with 20 canonical TAL

repeats, where each repeat comprises 34 amino acids (Fig. 1B, top inset). The N-terminal domain recognizes a TA DNA base pair, whereas each canonical TAL repeat recognizes a user-defined DNA base pair. The binding sequence that is recognized by each half of our staple proteins is thus 21 base pairs (bp) long. The inclusion of the N-terminal domain and the choice of 21-bp binding sequences were motivated by design simplicity (21 bp corresponds to two full turns of canonical B-form DNA) and also by results from biophysical affinity and sequence specificity studies (figs. S2 and S3). For example, ensemble fluorescence resonance energy transfer (FRET) measurements using green fluorescent protein (GFP)–TAL fusion proteins and Cyanine 3-labeled template DNA indicated bimolecular dissociation constants in the nanomolar regime (fig. S2). To test the sequence specificity of the TAL proteins, we performed gel shift–based competition assays, which revealed that a TAL protein with 20 repeats faithfully recognizes its correct sequence target in the presence of competing off-target DNA (fig. S3). In some cases, the TAL proteins were even able to discriminate a single mismatch base pair. We note that other researchers have reported similar specificity and selectivity tests in the meantime, with the purpose of creating improved TAL-effector nucleases (TALENs) for genome editing (37, 38).

To construct a double-TAL staple protein that can be genetically encoded in a single open reading frame for translation, we linked the C terminus of one DNA-recognizing TAL with the N terminus of another TAL (Fig. 1B, top inset). Given the absence of sufficiently detailed structural information about the N-terminal TAL domain and the properties of the C-terminal exit point, we had to design and experimentally test several different candidate peptide linker sequences (fig. S4A). On the basis of expression yield in *Escherichia coli*, solubility, and the ability to link two independent DNA double strands (fig. S4B), we selected one linker sequence out of 11 candidate sequences and used this linker in all staple proteins in this work. We also fused a GFP domain to the N terminus of the double-TAL staple protein. The fluorescence of GFP served to facilitate purification and analysis, and also acted as a placeholder for another protein domain with custom functionality.

To illustrate the shape of a double-TAL staple protein thus constructed and bound to two template double-helical DNA domains, we created a structural model consisting of two antiparallel DNA-bound TAL molecules (34) and calculated electron density projections from various directions (Fig. 1, C and D). The M-shaped projections agree well with the experimental realization of the antiparallel staple-protein connection in the context of larger DNA-protein hybrid structures as observed in electron microscopy experiments (Fig. 1, C and D).

Junction spacing rules

Having established the elementary double-TAL staple protein, we proceeded to identify a set of

Physics Department and Institute for Advanced Study, Technische Universität München, Garching bei München, Germany.

*Corresponding author. Email: dietz@tum.de

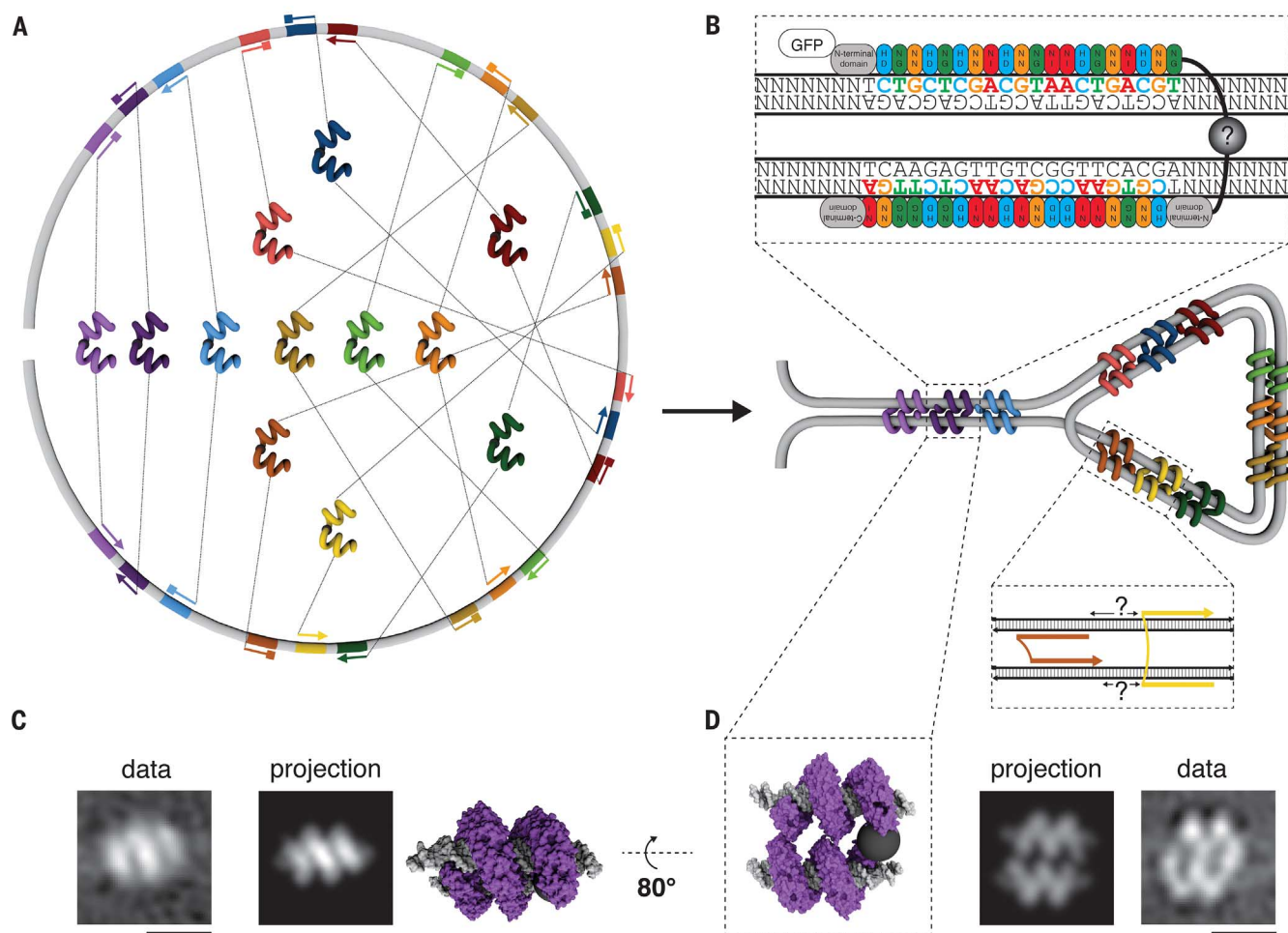


Fig. 1. A set of sequence-specific double-TAL staple proteins folds a double-stranded DNA template into a user-defined shape. (A) Schematic illustration of the design concept for constructing DNA-protein hybrid shapes. A double-stranded DNA template molecule (gray circle) contains several protein binding sites (colored segments) in different orientations and with defined spacing. Each double-TAL staple protein (helical models in center) specifically recognizes and connects two binding sites. (B) Schematic representation of the structure formed upon the self-assembly of the components shown in (A). Top inset: Composition of an exemplary double-TAL staple protein: two DNA binding motifs each consisting of a constant N-terminal domain and 20 repeat subunits, where each repeat recognizes individual base pairs in a sequence-specific fashion. Color coding indicates DNA base pair specificity of the individual repeats. To create a staple protein, we had to design and experimentally test several different candidate linkers (black line with question mark) to connect the two DNA binding

motifs. A GFP domain is fused to the N terminus of the staple protein and serves as a placeholder for various protein functionalities. Bottom inset: The correct spacing between two adjacent staple protein binding sites, here indicated with a question mark, is crucial for the planarity of the structure and was determined empirically in this work. (C) Right: Surface representation of a 3D model consisting of two copies of the crystal structure of a TAL effector (PDB: 3UGM). Center: Projection calculated from the model. Left: Reference-free class average (see fig. S8) of negative-stain transmission electron micrograph (TEM) images of double-TAL staple proteins bound to two parallel DNA double helices. (D) Model (left), projection (center), and data (right) as in (C), but in a different projection plane. Scale bars, 10 nm. The linker region of the staple protein is indicated as a black sphere in the models shown in (C) and (D), but it is not accounted for in the projections. See table S1 for an exemplary amino acid sequence of a double-TAL staple protein.

design rules for creating more complex structural frameworks based on multiple double TAL staple proteins and a long double-helical DNA template. A necessary step toward creating such more complex objects is the ability to connect two parallel helices by multiple staple proteins. Because of the helicity of B-form DNA, shifting one binding site relative to another on the same helix causes a rotation of one staple protein junction relative to the other. To obtain planarity, it is thus important to find suitable relative positions of the two binding sites on each DNA helix, which will de-

pend on the length of the double-helical spacer between the binding sites (Fig. 1B, bottom right inset). Because the binding sequence for a TAL protein can be contained in either of the two strands of a DNA double-helical domain, the TAL proteins can bind in different orientations. The relative orientation of the two adjacent staple proteins will affect the choice of suitable spacing between adjacent binding sites. In total, there are six unique relative orientations of two adjacent staple proteins (Fig. 2, A to D). In DNA nanotechnology, junction spacing rules are derived

from the geometry of B-form DNA (12, 14, 32). Here, the detailed geometrical properties of the staple protein connection were not available to us. For the configuration in which the adjacent TAL staple proteins have the same orientation (Fig. 2A), planarity is achieved by simply spacing the binding sites in integer multiples of a single B-form DNA helical turn. For the other five possible configurations, we had to determine empirically the junction spacing rules. On the basis of TEM imaging of a set of test structures (see fig. S5), we arrived at the spacing rules shown in Fig. 2.

The double-crossover motif in Fig. 2A features two staple proteins in the same orientation. The image obtained from the resulting structure resembles two copies of the antiparallel crossover motif from Fig. 1D, showing an MM-shaped signature on the top DNA double strand. By contrast,

the motif in Fig. 2B features two staple proteins in opposite orientations. The change in orientation is reflected in the resulting image, which now shows an MW-shaped signature on the top DNA double strand. Based on the spacer lengths, we again constructed structural models

and calculated electron density projections (Fig. 2, A and B). The projections agree well with the experimental image data and reproduce the subtle differences in the data from the different orientations.

The junction spacing rules shown in Fig. 2, A to D, enable construction of larger DNA-protein hybrid nanostructures, which may be achieved by combining multiple double crossover motifs such that staple proteins with the same orientations are spaced with distances corresponding to integer multiples of 21 bp. For example, the configuration in Fig. 2A may be simply repeated along the helical direction to form a filamentous two-helix bundle. Alternatively, the configuration in Fig. 2B may be used for the same purpose by alternating the spacer lengths (Fig. 2E).

To see whether some configurations may be preferable over others for creating larger hybrid objects, we constructed four distinct two-helix bundles using a set of 12 different staple proteins. For each two-helix bundle variant, we designed a custom DNA template sequence containing 24 unique recognition sites. We found that two-helix bundles built using repetitions of the double-crossover motifs in Fig. 2, A and D, tended to form multistranded higher-order structures, whereas the bundles based on the motifs in Fig. 2, B and C, remained mostly monomeric (fig. S6). We speculate that the highly repetitive patterns of TAL protein surface features can promote avidity effects in protein-protein interactions. This effect is strongly enhanced when all binding sites on one DNA double helix point into the same direction, as is the case for the double-crossover motifs in Fig. 2, A and D. Hence, to minimize the undesired repetitive interaction motifs, for further designs we used the alternating staple protein orientations from Fig. 2, B and C. To illustrate the site selectivity of our staple proteins, we incubated the template DNA used in the two-helix bundle shown in Fig. 2E with distinct subsets of the 12 staple proteins. The TEM data obtained from the resulting objects revealed binding of the staple proteins in the expected patterns (Fig. 2, F and G).

Structural motifs

Having established the fundamental design rules, we explored the possibility of creating structural modules such as custom curvatures, corners, and vertices. We designed a series of template DNA sequences that can be folded into different shapes by the same set of 12 staple proteins. We designed an 180° arc, an open circle, a closed ring, a three-armed star, a Drigalski spatula, a square, and a four-armed cross that will likely adopt a 3D tetrahedral shape (Fig. 3). Imaging of each object with TEM corroborated the successful assembly into the designed shape. The bent structures (Fig. 3, A to C) demonstrate that the staple proteins can bear mechanical loads. The closed ring and square objects (Fig. 3, C and F) were more homogeneous than the open objects, as expected because of the closure constraint. For the closed objects, we computed reference-free single-particle TEM class average images in which the individual

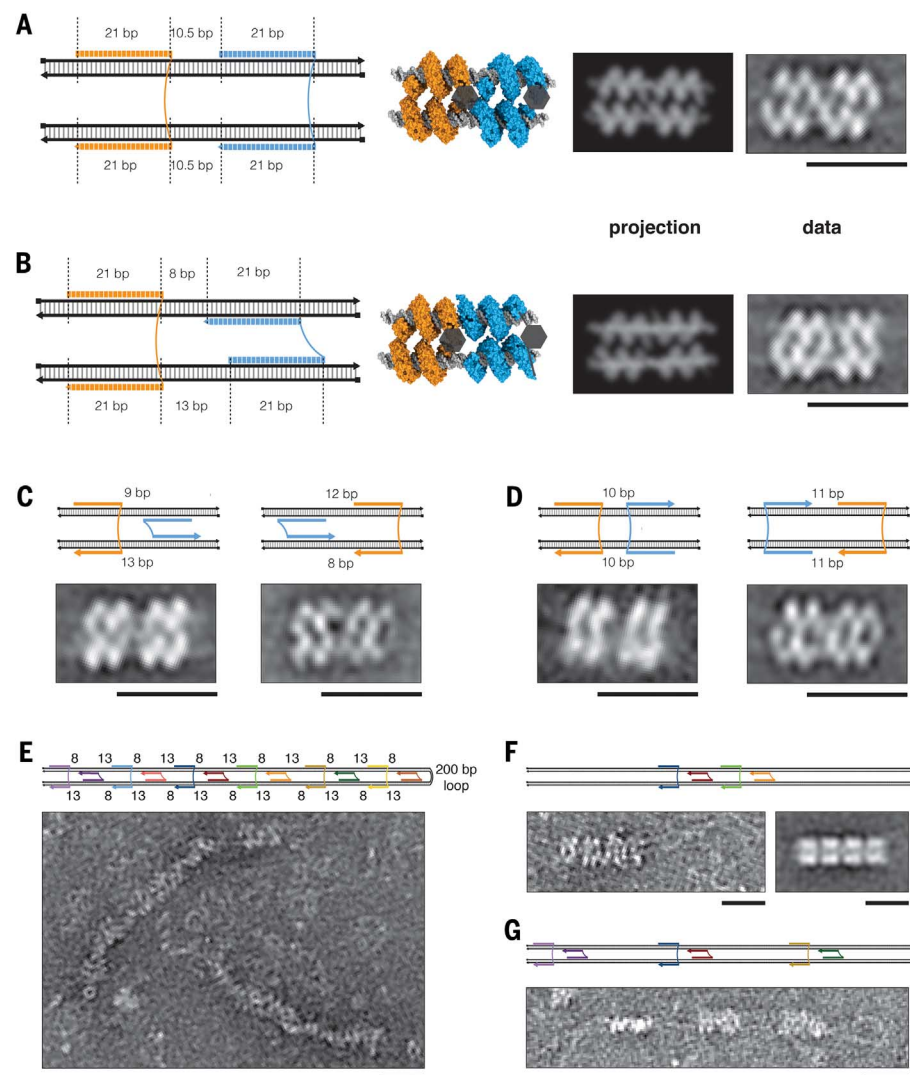


Fig. 2. Fundamental junction spacing rules for the design of DNA-protein hybrid nanostructures.

(A to D) Empirically derived optimal distances between binding sites in all six possible relative orientations of two adjacent double-TAL staple proteins. All binding sites are 21 bp long; spacers between binding sites are indicated by labels in the schematic representations. [(A) and (B)] From left to right: Schematic representation of two adjacent double-TAL staple proteins connecting two parallel DNA double helices; 3D model consisting of four copies of the crystal structure 3UGM (linker regions are indicated by black hexagons); projection calculated from the model (linker regions are not accounted for); class average of negative-stain TEM images of two adjacent double-TAL staple proteins connecting two parallel DNA double helices. [(C) and (D)] Schematic representations (top) and class averages (bottom) of two adjacent double-TAL staple proteins connecting two parallel DNA double helices. (E) Schematic representation (top) and single negative-stain TEM image (bottom) of a DNA-protein hybrid nanostructure consisting of a 1000-bp DNA double strand and 12 different double-TAL staple proteins. (F) Schematic representation (top), single negative-stain TEM image (bottom left), and class average (bottom right) of a DNA-protein hybrid nanostructure consisting of the same DNA double strand as the structure shown in (E) and four distinct staple proteins. (G) Schematic representation (top) and single negative-stain TEM image (bottom) of a DNA-protein hybrid nanostructure consisting of the same DNA double strand as the structures shown in (E) and (F) and six distinct staple proteins. Scale bars, 20 nm. See figs. S9 to S11 for field-of-view images of the objects shown in (E) to (G); see tables S2 and S3 for template sequences.

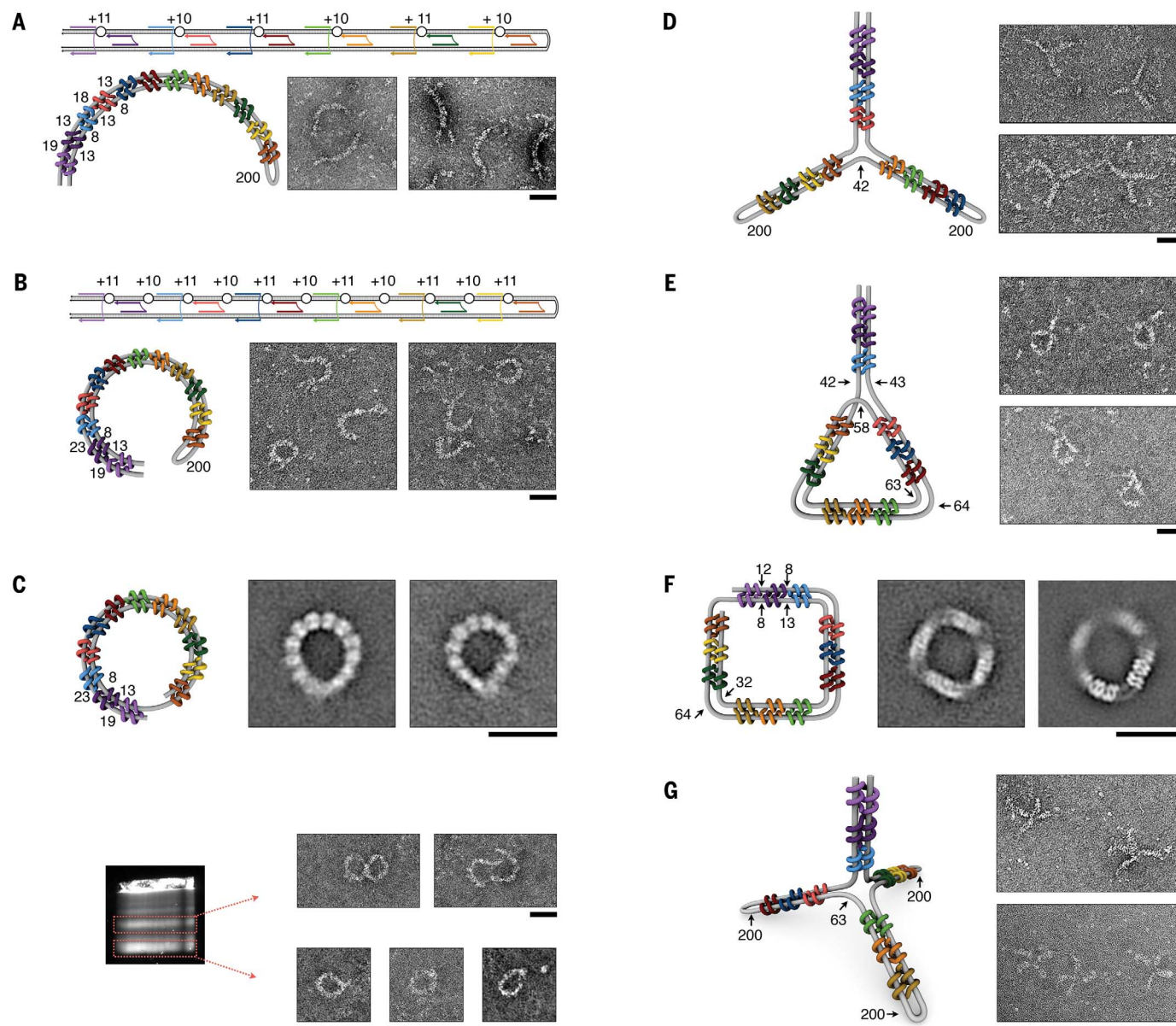


Fig. 3. Examples of single-layer DNA-protein hybrid nanostructures. (A and B) Schematic representations, both 2D (top) and 3D (bottom left), and single TEM images (bottom right) of bent versions of the two-helix bundle introduced in Fig. 2E. Curvature is induced by insertion of an additional 63 bp (A) or 116 bp (B) in one of the two parallel helices. (C) Top: Schematic representation (left) and averaged TEM micrographs (right) of a DNA-protein hybrid ring that exhibits the same curvature as the structure shown in (B) but is designed with a spiral-like routing of the double-stranded DNA template leading to ring closure. Bottom left: Laser scan (GFP channel, excitation 473 nm, emission 520 to 540 nm) of an agarose gel on which a self-assembly mixture of the hybrid ring was electrophoresed. Bottom right: Single TEM micro-

graphs of samples that were purified from the bands indicated with red boxes. (D and E) Schematic representation (left) and single TEM micrographs of a three-armed star (D) and a Drigalski spatula (E). (F) Schematic representation (left) and averaged TEM micrographs (right) of a DNA-protein hybrid square that was designed using the same spiral-like template routing as the ring in (C) but with additional spacers that are longer on one of the 12 helices, yielding corners instead of an evenly distributed curvature. (G) Schematic representation (left) and single TEM micrographs of a four-armed cross. Scale bars, 50 nm; labels indicate spacer lengths between protein binding sites. See Figs. S12 to S18 for field-of-view images; see tables S2 and S3 for template sequences.

staple proteins could be recognized. For the square object (Fig. 3F), one corner could be resolved in greater detail, revealing aspects of the staple proteins as well as of the two DNA template strands, which agreed with our design. The branched objects (Fig. 3, D, E, and G) were generally more flexible, but the topology reflected in the single-particle TEM images agreed with our

designs. The heterogeneous appearance of the four-armed cross particles (Fig. 3G) may be attributed to collapse of nonplanar tetrahedral conformations onto the 2D TEM imaging support.

Together, the objects in Fig. 3 constitute a set of design motifs that could be combined to create larger, more complex DNA-protein hybrid nanostructures. We also studied the objects in

agarose gel-electrophoretic mobility assays (Fig. 3C, bottom, and Fig. S6E). For example, the closed ring migrated in reasonably well-defined bands, and we could also purify the rings from such gels by physical extraction (Fig. 3C, bottom). The leading band corresponded to ring monomers; a slower second band corresponded to a dimeric species in which two template DNA molecules

appeared to be connected by the staple proteins, as seen by TEM imaging.

Multilayer structures

The objects with topological closure constraint appeared already relatively stiff. Alternatively, enhanced structural rigidity of target objects can also be achieved by connecting multiple layers of parallel helices. To test for the possibility of creating staple protein connections that are compatible with 2D helix packing, we designed a DNA template sequence for a four-helix bundle with a 2×2 helix cross section (Fig. 4A). To create the necessary staple protein connections compatible with linkages pointing to multiple

neighboring helices, we modified the spacer design configuration from Fig. 2B. To prevent steric conflicts from packing, we increased the overall distance between staple proteins. Additionally, we also shifted every second binding site to induce a relative orientation of adjacent crossovers of $\sim 90^\circ$ based on B-form DNA geometry (Fig. 4A). The four-helix bundle thus designed successfully self-assembled at room temperature from a mixture containing the designed template DNA and the 12 unique staple proteins introduced above. TEM imaging revealed rod-like particles (Fig. 4C) with the expected pattern of six segments produced by the transmission projection of the double layer of TAL staple proteins, in-

dicating that the structures folded as designed. As expected, the four-helix DNA-protein rods exhibited greater shape homogeneity relative to the two-helix objects lacking a closure constraint, which we attribute to the desired greater bending stiffness caused by the multilayer design.

Classifying and averaging individual particle micrographs of the four-helix bundle revealed a number of dominant transmission views with distinct thickness of the rod particles in the image plane (Fig. 4C). To understand the appearance of the particles, we constructed a structural model for a segment of our four-helix bundle based on the rhombohedral crystal packing of TAL effectors, as seen in x-ray diffraction experiments (34) and computed electron density projections (Fig. 4D). The computed projections reproduced the thickness variation that we observed in our TEM data. We expect that the flexible linkers in the staple proteins allow the structure to relax into a conformation in which protein-protein interactions also are optimized. Given the correspondence of our TEM data with the computed projections (Fig. 4C versus Fig. 4D), we consider it likely that the four-helix bundle adopts a configuration that resembles the crystal packing of TAL effectors, leading to a diamond-shaped cross section in the helical direction of the four-helix bundle.

Considering also the pronounced tendency to form higher-order structures when using repetitive TAL protein orientations that we observed in several single-layer structures (see fig. S6), we thus conclude that the TAL staple proteins provide additional interaction surfaces that further stabilize the DNA-protein hybrid nanostructures internally, beyond the rotationally unconstrained peptide linker in each staple protein. However, although the packing of the helices appears to be governed by optimizing protein-protein interactions, the global shape of the four-helix bundle is controlled by the designed sequence of the double-helical DNA template. To demonstrate this fact, we prepared a curved variant of the four-helix bundle (Fig. 4E). The curvature was achieved by inserting additional base pairs between adjacent staple protein binding sites in two out of the four helices. TEM imaging confirmed that the curved four-helix bundle self-assembled successfully from the template DNA thus modified and the same set of 12 staple proteins that was used for the straight variant.

Genetically encoded self-assembly

Finally, we tested the possibility for self-assembly at physiological conditions of our DNA-protein hybrid nanostructures starting from genetic expression (Fig. 5). To this end, we used an *in vitro* expression one-pot mixture comprising RNA polymerase, ribosomes, and the various auxiliary co-factors that are necessary for transcription and translation, such as nucleotides, amino acids, transfer RNAs (tRNAs), tRNA transferases, etc. To this mixture, we added a template strand for a hybrid nanostructure and 12 different plasmids featuring the genes for 12 different double-TAL staple proteins. After 6 hours of incubation at 25°C ,

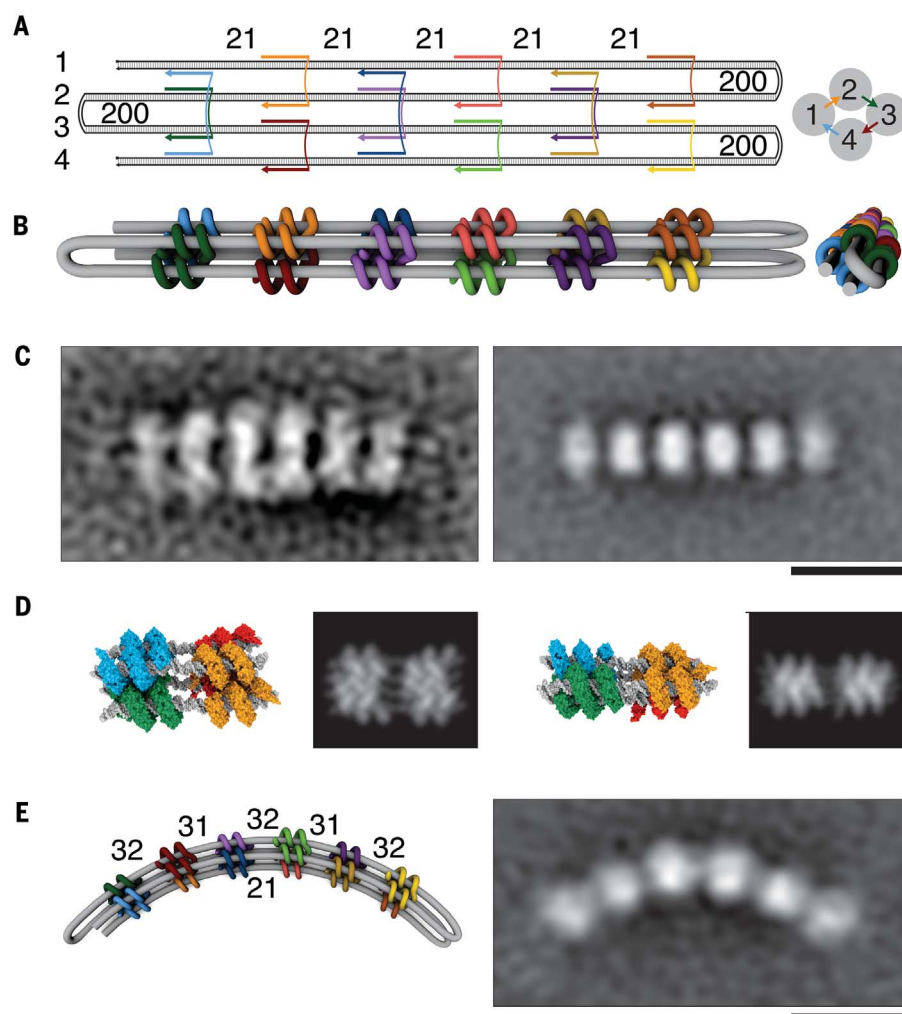


Fig. 4. Examples of multilayer DNA-protein hybrid nanostructures. (A and B) Schematic representations, both 2D (A) and 3D (B), of a straight four-helix bundle comprising a 1750-bp DNA double strand and 12 different double-TAL staple proteins. Loops between parallel helices each consist of 200 bp. Spacers between binding sequences have been adjusted to rotate by $\sim 90^\circ$ every second crossover. (C) Averaged TEM micrographs of the straight four-helix bundle. (D) Model consisting of eight copies of the crystal structure 3UGM and projections derived from the model. Different rotational orientations of the model give rise to projections of different aspect ratios that match the experimental data shown in (C). (E) Schematic representation (left) and averaged TEM micrographs (right) of a bent four-helix bundle. Curvature is induced by insertion of an additional 106 bp distributed along helices 2 and 3, as indicated by the labels. Scale bars, 50 nm. See figs. S19 to S22 for field-of-view images and exemplary particle libraries; see tables S2 and S3 for template sequences.

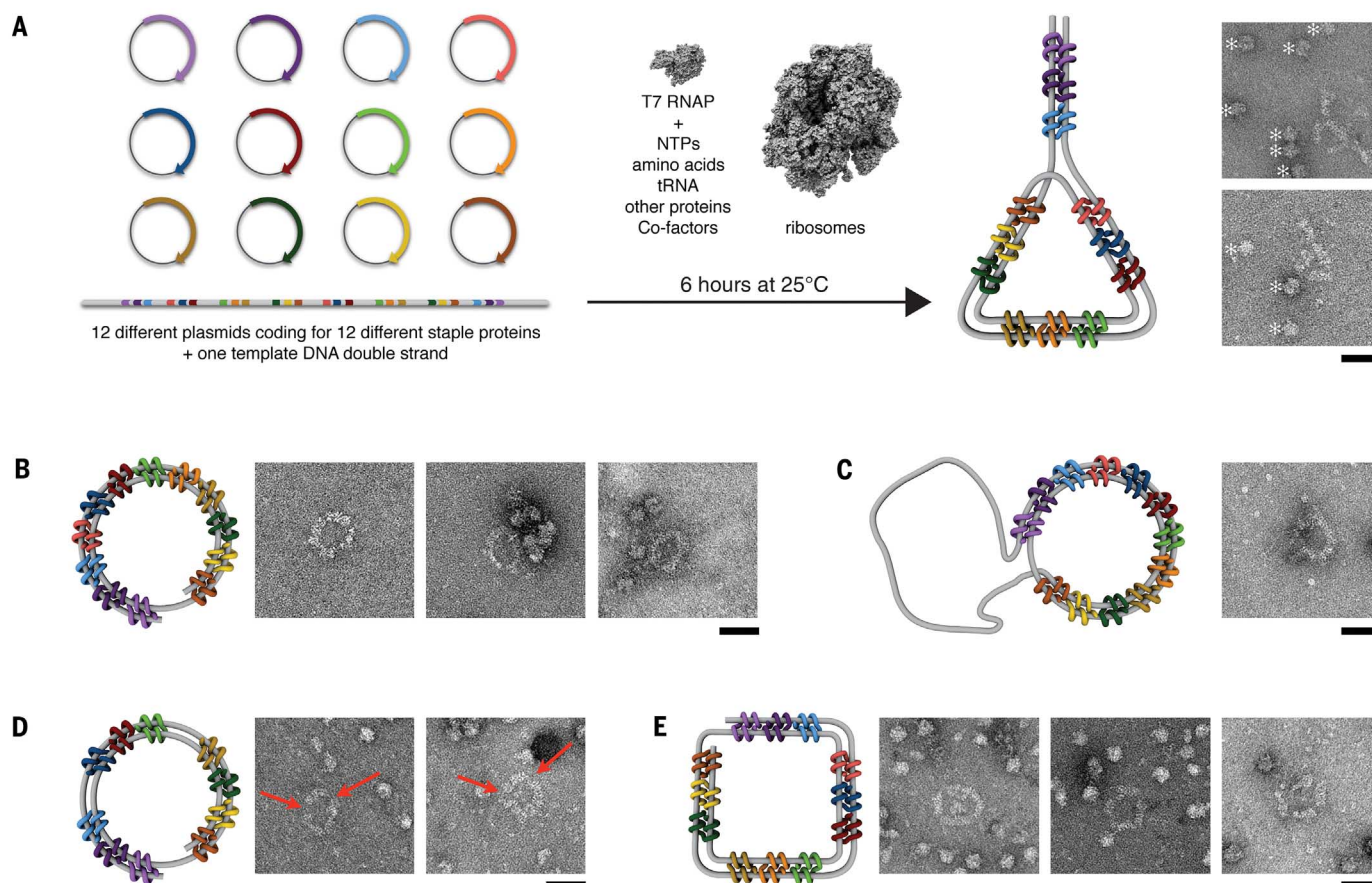


Fig. 5. Self-assembly of genetically expressed DNA-protein hybrid nanostructures. (A) A set of 12 different plasmids containing the genes for 12 different staple proteins and a template DNA double strand (left) are incubated with a cell-free transcription and translation mixture (PURExpress, NEB). The mixture contains T7 RNA polymerase (PDB: 1MSW), which transcribes the genes into mRNA, and *E. coli* ribosomes (PDB: 5LZE), which translate the mRNA into the 12 different staple proteins. The staple proteins can then fold the template strand into the designed shape, in this case a Drigalski spatula (right). TEM micrographs show assembled hybrid nanostructures as well as ribosomes (indicated by asterisks) and other components of the expression mixture. For imaging, all samples were diluted 1000- to 10,000-fold in either

phosphate-buffered saline or a buffer containing 50 mM Tris, 100 mM NaCl, and 10 mM MgCl₂ (pH 8.5), where the addition of Mg²⁺ improved the particle density on the TEM grid. (B and C) Schematic representation and single TEM micrographs of a hybrid ring that was assembled using either a linear template strand (B) or a circular plasmid as a template (C). (D) Schematic representation and single TEM micrographs of a hybrid ring that was assembled using either a linear template strand in a mixture containing only 10 of the 12 different plasmids. Gaps caused by the absence of two staple proteins are indicated with red arrows. (E) Schematic representation and single TEM micrographs of a hybrid square that was cotranslationally assembled. Scale bars, 50 nm.

intact self-assembled DNA-protein hybrid nanostructures emerged and could be discerned side-by-side with ribosomes and other components in TEM images acquired from the self-assembly reaction mixtures. To verify (as in Fig. 2, F and G) the site specificity of staple protein binding, we used only 10 of the 12 double-TAL staple genes in combination with the template for the hybrid ring. TEM imaging revealed that the structures formed in this reaction mixture, as expected, contained gaps at the binding sites for the two staple proteins that were excluded (Fig. 5D, red arrows).

Discussion

In this study, we developed design rules for creating custom single-layer and multilayer DNA-protein hybrid nanostructures; using these rules, we successfully self-assembled 18 distinct objects.

We have observed a tendency for aggregation that we attribute to protein-protein interactions. In the future, the rational reengineering of the TAL surfaces using computational protein design (39) may enable suppression of unwanted interactions in TAL repeats at the outside of assembled objects while preserving those interactions that stabilize the objects internally. We have used linear polymerase chain reaction (PCR) products as template DNA to produce the majority of the objects shown in Figs. 1 to 5, but circular plasmids may be used just as well (Fig. 5C, fig. S6, E and F, and fig. S7). Thus, all of the components needed for the assembly of our hybrid nanostructures can be encoded genetically. Moreover, the assembly of our structures proceeds upon simple mixing at room temperature at near-physiological buffer conditions, which allows for self-assembly after transcription of

the genes, as we demonstrated in Fig. 5. In vivo assembly of our DNA-protein hybrid nanostructures appears thus a realistic possibility.

Regarding the integration of multiple functionalities, additional protein domains may be readily fused to the staple proteins by conventional protein engineering methods to arrange these groups in a user-defined 3D spatial arrangement. In our experiments, each staple protein already carried a placeholder for such a protein domain with user-defined functionality, as represented by GFP domains fused to the N termini of the double-TAL staple proteins.

In our experiments, we created a diversity of structures by designing custom DNA template sequences while reusing a set of 12 unique staple proteins. Redesigning the template DNA sequences while reusing, for example, our set of 12 staple proteins is convenient in that it only

requires gene synthesis. However, given the programmability of TAL proteins, a virtually unlimited number of staple proteins could be created. Designing additional double-TAL staple proteins may be implemented with efficient TAL cloning methods (40, 41), which is also the approach that we adopted initially to create the 12 unique double-TAL staple proteins. Designing a set of custom staple proteins in order to fold a given target DNA double strand into a desired shape could be of interest, for example, as a means of rationally creating custom structures and loops in cellular genomes to dissect the influence of genome looping on gene regulation (7).

Many current applications of bottom-up nanotechnology, and DNA nanotechnology in particular, rely on positioning or displaying of a few target features, often proteins, with multiple nanometer accuracy (27, 42–44). Custom DNA-based tools have fueled scientific discovery for example by supporting the study of the collective behavior of molecular motors (43), the influence of ligand spacing on receptor binding (42), and elementary biomolecular interactions (45, 46). Arranging antibodies and other functional groups on DNA backbone objects has been considered for smarter therapeutics (27), and scaffolding the enzymes involved in a biosynthetic pathway appears a promising route for efficient production of target compounds in industrial biotechnology (47). All these applications face technical hurdles with respect to integrating in particular protein components at user defined positions, to producing such objects at quantities required for organism-scale applications, and to using such objects inside cells. Our approach for creating DNA-protein hybrid nanostructures affords attractive capabilities with respect to positioning target features in custom nanoscale frameworks, and offers the additional advantage that all structural components, and potentially also the fully assembled objects including the functional protein groups, may be produced in cells. Apart from the possibility for scalable mass production and the ease of integrating other functional proteins by terminal fusions to the double-TAL staple proteins, our method could therefore enable in vivo applications that so far have not been amenable to current methods in nanotechnology.

Materials and methods

We designed our objects using the procedure detailed in fig. S1.

Cloning

All TAL expression constructs were assembled from a library of individual TAL repeats using Golden-Gate cloning. We constructed our own library based on previous work by Cermak *et al.* (40) and Zhang *et al.* (41). We adapted the library to allow assembly of TAL constructs with different lengths and of double-TAL staple proteins with different linker sequences. For sequences of the expression plasmids, see tables S4 to S15. Expression plasmids and selected templates will be made available at ADDGENE.

Expression and purification

Expression was performed in Rosetta 2 DE3 cells for 20 hours at 16°C. Proteins were purified using Ni-NTA agarose beads (31) and either stored at 4°C for up to 2 weeks or frozen in liquid nitrogen and stored at –80°C. Protein concentration was determined from absorbance spectra recorded at a pathlength of 10 mm using the extinction coefficient of cycle3-GFP at 397 nm of 30,000 M^{–1} cm^{–1} (48).

Assembly of DNA-protein hybrid nanostructures

All template sequences were synthesized by Eurofins Genomics (Ebersberg, Germany) and delivered in a standard plasmid backbone (pEX-A2 or pEX-K4). Linear dsDNA templates were produced by PCR using primers that bind in the plasmid backbone yielding template strands with approximately 100- to 130-bp overhangs before the first and after the last binding sequence, respectively. Assembly of hybrid nanostructures was performed by mixing the template DNA at concentrations between 5 and 20 nM with a 4-fold excess per staple protein over template DNA using a solution of pre-mixed staple proteins, and incubating for one to four hours at room temperature.

TEM imaging and image processing

Samples were diluted to final concentrations between 0.5 and 2 nM and adsorbed on glow-discharged Formvar-supported carbon-coated Cu400 TEM grids (Science Services, Munich) and stained using a 2% aqueous uranyl formate solution containing 25 mM NaOH. Imaging was performed using either a Philips CM100 EM operated at 100 kV or a FEI Tecnai Spirit operated at 120 kV. Reference-free class averaging and calculation of projections from 3D models was performed using Xmipp 3.0 (49). Models based on the crystal structure were constructed using UCSF Chimera (50). TEM micrographs were subjected to bilinear downsampling (ImageJ), high-pass filtering to remove long-range staining gradients, sharpening to enhance particle edges, and contrast auto-leveling (Adobe Photoshop CS5).

Gel electrophoresis of DNA-protein hybrid nanostructures

Hybrid nanostructures were assembled as described above and electrophoresed in a 1.5% agarose gel, in an ice bath. After scanning the gel in a Typhoon FLA 9500 laser scanner (GE), the desired bands were cut out and applied to a 0.45 µm spin filter. After centrifugation for 5 min at 5000 rcf (4°C) the filtrate was immediately applied to Formvar-supported carbon-coated Cu400 TEM grids and stained as described above.

One-pot in vitro expression and self-assembly of DNA-protein hybrid nanostructures

For in vitro expression, the PURExpress system (New England Biolabs) was used. Reactions with a final volume of 25 µl contained 10 µl solution A,

7.5 µl solution B, 1 µl murine RNase inhibitor (New England Biolabs), 1080 ng plasmids (12 plasmids @ 90 ng per plasmid), and 5 nM template DNA. Reaction mixtures were incubated at 25°C for 6–8 hours, diluted 1,000–10,000 fold and immediately applied to TEM grids and stained as described above.

REFERENCES AND NOTES

1. S. S. Rao *et al.*, A 3D map of the human genome at kilobase resolution reveals principles of chromatin looping. *Cell* **159**, 1665–1680 (2014). doi: [10.1016/j.cell.2014.11.021](https://doi.org/10.1016/j.cell.2014.11.021); pmid: [25497547](https://pubmed.ncbi.nlm.nih.gov/25497547/)
2. C. J. Bashor, N. C. Helman, S. Yan, W. A. Lim, Using engineered scaffold interactions to reshape MAP kinase pathway signaling dynamics. *Science* **319**, 1539–1543 (2008). doi: [10.1126/science.1151153](https://doi.org/10.1126/science.1151153); pmid: [18339942](https://pubmed.ncbi.nlm.nih.gov/18339942/)
3. M. C. Good, J. G. Zalatan, W. A. Lim, Scaffold proteins: Hubs for controlling the flow of cellular information. *Science* **332**, 680–686 (2011). doi: [10.1126/science.1198701](https://doi.org/10.1126/science.1198701); pmid: [21551057](https://pubmed.ncbi.nlm.nih.gov/21551057/)
4. R. J. Conrado, J. D. Varner, M. P. DeLisa, Engineering the spatial organization of metabolic enzymes: Mimicking nature's synergy. *Curr. Opin. Biotechnol.* **19**, 492–499 (2008). doi: [10.1016/j.copbio.2008.07.006](https://doi.org/10.1016/j.copbio.2008.07.006); pmid: [18725290](https://pubmed.ncbi.nlm.nih.gov/18725290/)
5. H. M. Berman *et al.*, The Protein Data Bank. *Nucleic Acids Res.* **28**, 235–242 (2000). doi: [10.1093/nar/28.1.235](https://doi.org/10.1093/nar/28.1.235); pmid: [10592235](https://pubmed.ncbi.nlm.nih.gov/10592235/)
6. N. Koga *et al.*, Principles for designing ideal protein structures. *Nature* **491**, 222–227 (2012). doi: [10.1038/nature11600](https://doi.org/10.1038/nature11600); pmid: [23135467](https://pubmed.ncbi.nlm.nih.gov/23135467/)
7. B. E. Correia *et al.*, Proof of principle for epitope-focused vaccine design. *Nature* **507**, 201–206 (2014). doi: [10.1038/nature12966](https://doi.org/10.1038/nature12966); pmid: [24499818](https://pubmed.ncbi.nlm.nih.gov/24499818/)
8. S. J. Fleishman *et al.*, Computational design of proteins targeting the conserved stem region of influenza hemagglutinin. *Science* **332**, 816–821 (2011). doi: [10.1126/science.1202617](https://doi.org/10.1126/science.1202617); pmid: [21566186](https://pubmed.ncbi.nlm.nih.gov/21566186/)
9. N. P. King *et al.*, Accurate design of co-assembling multi-component protein nanomaterials. *Nature* **510**, 103–108 (2014). doi: [10.1038/nature13404](https://doi.org/10.1038/nature13404); pmid: [24870237](https://pubmed.ncbi.nlm.nih.gov/24870237/)
10. A. R. Thomson *et al.*, Computational design of water-soluble α -helical barrels. *Science* **346**, 485–488 (2014). doi: [10.1126/science.1257452](https://doi.org/10.1126/science.1257452); pmid: [25342807](https://pubmed.ncbi.nlm.nih.gov/25342807/)
11. M. R. Jones, N. C. Seeman, C. A. Mirkin, Programmable materials and the nature of the DNA bond. *Science* **347**, 1260901 (2015). doi: [10.1126/science.1260901](https://doi.org/10.1126/science.1260901); pmid: [25700524](https://pubmed.ncbi.nlm.nih.gov/25700524/)
12. P. W. Rothmund, Folding DNA to create nanoscale shapes and patterns. *Nature* **440**, 297–302 (2006). doi: [10.1038/nature04586](https://doi.org/10.1038/nature04586); pmid: [16541064](https://pubmed.ncbi.nlm.nih.gov/16541064/)
13. S. M. Douglas *et al.*, Self-assembly of DNA into nanoscale three-dimensional shapes. *Nature* **459**, 414–418 (2009). doi: [10.1038/nature08016](https://doi.org/10.1038/nature08016); pmid: [19458720](https://pubmed.ncbi.nlm.nih.gov/19458720/)
14. H. Dietz, S. M. Douglas, W. M. Shih, Folding DNA into twisted and curved nanoscale shapes. *Science* **325**, 725–730 (2009). doi: [10.1126/science.1174251](https://doi.org/10.1126/science.1174251); pmid: [19661424](https://pubmed.ncbi.nlm.nih.gov/19661424/)
15. Y. Ke, L. L. Ong, W. M. Shih, P. Yin, Three-dimensional structures self-assembled from DNA bricks. *Science* **338**, 1177–1183 (2012). doi: [10.1126/science.1227268](https://doi.org/10.1126/science.1227268); pmid: [23197527](https://pubmed.ncbi.nlm.nih.gov/23197527/)
16. D. Han *et al.*, DNA gridiron nanostructures based on four-arm junctions. *Science* **339**, 1412–1415 (2013). doi: [10.1126/science.1232252](https://doi.org/10.1126/science.1232252); pmid: [23520107](https://pubmed.ncbi.nlm.nih.gov/23520107/)
17. E. Benson *et al.*, DNA rendering of polyhedral meshes at the nanoscale. *Nature* **523**, 441–444 (2015). doi: [10.1038/nature14586](https://doi.org/10.1038/nature14586); pmid: [26201596](https://pubmed.ncbi.nlm.nih.gov/26201596/)
18. J. Zheng *et al.*, From molecular to macroscopic via the rational design of a self-assembled 3D DNA crystal. *Nature* **461**, 74–77 (2009). doi: [10.1038/nature08274](https://doi.org/10.1038/nature08274); pmid: [19727196](https://pubmed.ncbi.nlm.nih.gov/19727196/)
19. Y. Suzuki, M. Endo, H. Sugiyama, Lipid-bilayer-assisted two-dimensional self-assembly of DNA origami nanostructures. *Nat. Commun.* **6**, 8052 (2015). doi: [10.1038/ncomms9052](https://doi.org/10.1038/ncomms9052); pmid: [26310995](https://pubmed.ncbi.nlm.nih.gov/26310995/)
20. A. Aghebat Rafat, T. Pirzer, M. B. Scheible, A. Kostina, F. C. Simmel, Surface-assisted large-scale ordering of DNA origami tiles. *Angew. Chem. Int. Ed.* **53**, 7665–7668 (2014). doi: [10.1002/anie.201403965](https://doi.org/10.1002/anie.201403965); pmid: [24894973](https://pubmed.ncbi.nlm.nih.gov/24894973/)
21. E. Winfree, F. Liu, L. A. Wenzler, N. C. Seeman, Design and self-assembly of two-dimensional DNA crystals. *Nature* **394**, 539–544 (1998). doi: [10.1038/28998](https://doi.org/10.1038/28998); pmid: [9707114](https://pubmed.ncbi.nlm.nih.gov/9707114/)

22. T. Gerling, K. F. Wagenbauer, A. M. Neuner, H. Dietz, Dynamic DNA devices and assemblies formed by shape-complementary, non-base pairing 3D components. *Science* **347**, 1446–1452 (2015). doi: [10.1126/science.aaa5372](https://doi.org/10.1126/science.aaa5372); pmid: [25814577](https://pubmed.ncbi.nlm.nih.gov/25814577/)
23. P. Ketterer, E. M. Willner, H. Dietz, Nanoscale rotary apparatus formed from tight-fitting 3D DNA components. *Sci. Adv.* **2**, e1501209 (2016). doi: [10.1126/sciadv.1501209](https://doi.org/10.1126/sciadv.1501209); pmid: [26989778](https://pubmed.ncbi.nlm.nih.gov/26989778/)
24. A. E. Marras, L. Zhou, H. J. Su, C. E. Castro, Programmable motion of DNA origami mechanisms. *Proc. Natl. Acad. Sci. U.S.A.* **112**, 713–718 (2015). doi: [10.1073/pnas.1408869112](https://doi.org/10.1073/pnas.1408869112); pmid: [25561550](https://pubmed.ncbi.nlm.nih.gov/25561550/)
25. Y. Liu, C. Lin, H. Li, H. Yan, Aptamer-directed self-assembly of protein arrays on a DNA nanostructure. *Angew. Chem. Int. Ed.* **44**, 4333–4338 (2005). doi: [10.1002/anie.200501089](https://doi.org/10.1002/anie.200501089); pmid: [15945116](https://pubmed.ncbi.nlm.nih.gov/15945116/)
26. H. Yan, S. H. Park, G. Finkelstein, J. H. Reif, T. H. LaBean, DNA-templated self-assembly of protein arrays and highly conductive nanowires. *Science* **301**, 1882–1884 (2003). doi: [10.1126/science.1089389](https://doi.org/10.1126/science.1089389); pmid: [14512621](https://pubmed.ncbi.nlm.nih.gov/14512621/)
27. S. M. Douglas, I. Bachelet, G. M. Church, A logic-gated nanorobot for targeted transport of molecular payloads. *Science* **335**, 831–834 (2012). doi: [10.1126/science.1214081](https://doi.org/10.1126/science.1214081); pmid: [22344439](https://pubmed.ncbi.nlm.nih.gov/22344439/)
28. Y. Mou, J. Y. Yu, T. M. Wannier, C. L. Guo, S. L. Mayo, Computational design of co-assembling protein-DNA nanowires. *Nature* **525**, 230–233 (2015). doi: [10.1038/nature14874](https://doi.org/10.1038/nature14874); pmid: [26331548](https://pubmed.ncbi.nlm.nih.gov/26331548/)
29. J. P. Sobczak, T. G. Martin, T. Gerling, H. Dietz, Rapid folding of DNA into nanoscale shapes at constant temperature. *Science* **338**, 1458–1461 (2012). doi: [10.1126/science.1229919](https://doi.org/10.1126/science.1229919); pmid: [23239734](https://pubmed.ncbi.nlm.nih.gov/23239734/)
30. C. Geary, P. W. Rothmund, E. S. Andersen, A single-stranded architecture for cotranscriptional folding of RNA nanostructures. *Science* **345**, 799–804 (2014). doi: [10.1126/science.1253920](https://doi.org/10.1126/science.1253920); pmid: [25124436](https://pubmed.ncbi.nlm.nih.gov/25124436/)
31. See supplementary materials.
32. T. J. Fu, N. C. Seeman, DNA double-crossover molecules. *Biochemistry* **32**, 3211–3220 (1993). doi: [10.1021/bi00064a003](https://doi.org/10.1021/bi00064a003); pmid: [8461289](https://pubmed.ncbi.nlm.nih.gov/8461289/)
33. J. Boch et al., Breaking the code of DNA binding specificity of TAL-type III effectors. *Science* **326**, 1509–1512 (2009). doi: [10.1126/science.1178811](https://doi.org/10.1126/science.1178811); pmid: [19933107](https://pubmed.ncbi.nlm.nih.gov/19933107/)
34. A. N. S. Mak, P. Bradley, R. A. Cernadas, A. J. Bogdanove, B. L. Stoddard, The crystal structure of TAL effector PthXo1 bound to its DNA target. *Science* **335**, 716–719 (2012). doi: [10.1126/science.1216211](https://doi.org/10.1126/science.1216211); pmid: [22223736](https://pubmed.ncbi.nlm.nih.gov/22223736/)
35. D. Deng et al., Structural basis for sequence-specific recognition of DNA by TAL effectors. *Science* **335**, 720–723 (2012). doi: [10.1126/science.1215670](https://doi.org/10.1126/science.1215670); pmid: [22223738](https://pubmed.ncbi.nlm.nih.gov/22223738/)
36. H. Gao, X. Wu, J. Chai, Z. Han, Crystal structure of a TALE protein reveals an extended N-terminal DNA binding region. *Cell Res.* **22**, 1716–1720 (2012). doi: [10.1038/cr.2012.156](https://doi.org/10.1038/cr.2012.156); pmid: [23147789](https://pubmed.ncbi.nlm.nih.gov/23147789/)
37. J. F. Meckler et al., Quantitative analysis of TALE-DNA interactions suggests polarity effects. *Nucleic Acids Res.* **41**, 4118–4128 (2013). pmid: [23408851](https://pubmed.ncbi.nlm.nih.gov/23408851/)
38. M. L. Christian et al., Targeting G with TAL effectors: A comparison of activities of TALENs constructed with NN and NK repeat variable di-residues. *PLOS ONE* **7**, e45383 (2012). doi: [10.1371/journal.pone.0045383](https://doi.org/10.1371/journal.pone.0045383); pmid: [23028976](https://pubmed.ncbi.nlm.nih.gov/23028976/)
39. T. J. Brunette et al., Exploring the repeat protein universe through computational protein design. *Nature* **528**, 580–584 (2015). doi: [10.1038/nature16162](https://doi.org/10.1038/nature16162); pmid: [26675729](https://pubmed.ncbi.nlm.nih.gov/26675729/)
40. T. Cermak et al., Efficient design and assembly of custom TALEN and other TAL effector-based constructs for DNA targeting. *Nucleic Acids Res.* **39**, e82 (2011). doi: [10.1093/nar/gkr218](https://doi.org/10.1093/nar/gkr218); pmid: [21493687](https://pubmed.ncbi.nlm.nih.gov/21493687/)
41. F. Zhang et al., Efficient construction of sequence-specific TAL effectors for modulating mammalian transcription. *Nat. Biotechnol.* **29**, 149–153 (2011). doi: [10.1038/nbt.1775](https://doi.org/10.1038/nbt.1775); pmid: [21248753](https://pubmed.ncbi.nlm.nih.gov/21248753/)
42. A. Shaw et al., Spatial control of membrane receptor function using ligand nanocalipers. *Nat. Methods* **11**, 841–846 (2014). doi: [10.1038/nmeth.3025](https://doi.org/10.1038/nmeth.3025); pmid: [24997862](https://pubmed.ncbi.nlm.nih.gov/24997862/)
43. N. D. Derr et al., Tug-of-war in motor protein ensembles revealed with a programmable DNA origami scaffold. *Science* **338**, 662–665 (2012). doi: [10.1126/science.1226734](https://doi.org/10.1126/science.1226734); pmid: [23065903](https://pubmed.ncbi.nlm.nih.gov/23065903/)
44. J. J. Funke, H. Dietz, Placing molecules with Bohr radius resolution using DNA origami. *Nat. Nanotechnol.* **11**, 47–52 (2016). doi: [10.1038/nnano.2015.240](https://doi.org/10.1038/nnano.2015.240); pmid: [26479026](https://pubmed.ncbi.nlm.nih.gov/26479026/)
45. F. Kilchherr et al., Single-molecule dissection of stacking forces in DNA. *Science* **353**, aaf5508 (2016). doi: [10.1126/science.aaf5508](https://doi.org/10.1126/science.aaf5508); pmid: [27609897](https://pubmed.ncbi.nlm.nih.gov/27609897/)
46. J. J. Funke et al., Uncovering the forces between nucleosomes using DNA origami. *Sci. Adv.* **2**, e1600974 (2016). pmid: [28138524](https://pubmed.ncbi.nlm.nih.gov/28138524/)
47. M. Liu et al., A three-enzyme pathway with an optimised geometric arrangement to facilitate substrate transfer. *ChemBioChem* **17**, 1097–1101 (2016). doi: [10.1002/cbic.201600103](https://doi.org/10.1002/cbic.201600103); pmid: [26995014](https://pubmed.ncbi.nlm.nih.gov/26995014/)
48. G. H. Patterson, S. M. Knobel, W. D. Sharif, S. R. Kain, D. W. Piston, Use of the green fluorescent protein and its mutants in quantitative fluorescence microscopy. *Biophys. J.* **73**, 2782–2790 (1997). doi: [10.1016/S0006-3495\(97\)78307-3](https://doi.org/10.1016/S0006-3495(97)78307-3); pmid: [9370472](https://pubmed.ncbi.nlm.nih.gov/9370472/)
49. S. H. Scheres, R. Núñez-Ramírez, C. O. Sorzano, J. M. Carazo, R. Marabini, Image processing for electron microscopy single-particle analysis using XMIPP. *Nat. Protoc.* **3**, 977–990 (2008). doi: [10.1038/nprot.2008.62](https://doi.org/10.1038/nprot.2008.62); pmid: [18536645](https://pubmed.ncbi.nlm.nih.gov/18536645/)
50. E. F. Pettersen et al., UCSF Chimera—a visualization system for exploratory research and analysis. *J. Comput. Chem.* **25**, 1605–1612 (2004). doi: [10.1002/jcc.20084](https://doi.org/10.1002/jcc.20084); pmid: [15264254](https://pubmed.ncbi.nlm.nih.gov/15264254/)

ACKNOWLEDGMENTS

We thank S. Ständer, M. Honemann, and J. Valtin for technical assistance, K. Wagenbauer for help with TEM imaging, and T. Gerling and E. Stahl for discussions. Supported by European Research Council starting grant 256270 (H.D.), Bundesministerium für Bildung und Forschung grant 031 A 458, and the Deutsche Forschungsgemeinschaft through grants provided within the Gottfried-Wilhelm-Leibniz Program and the Excellence Cluster CIPSM (Center for Integrated Protein Science Munich). All data are reported in the main text and supplement.

SUPPLEMENTARY MATERIALS

www.sciencemag.org/content/355/6331/eaam5488/suppl/DC1
Materials and Methods
Figs. S1 to S22
Tables S1 to S15
hybrid_structure_generator.xlsx file

7 December 2016; accepted 13 February 2017
10.1126/science.aam5488

Self-assembly of genetically encoded DNA-protein hybrid nanoscale shapes

Florian Praetorius and Hendrik Dietz

Science **355** (6331), eaam5488.
DOI: 10.1126/science.aam5488

Protein-folded DNA nanostructures

A wide variety of DNA nanostructures have been assembled by folding long DNA single strands with short DNA staples. However, such structures typically need annealing at elevated temperatures in order to form. To accommodate the formation of such structures in living cells, Praetorius and Dietz developed an approach in which custom protein staples based on transcription activator–like effector proteins fold double-stranded DNA templates (see the Perspective by Douglas). The structures folded into user-defined geometric shapes on the scale of tens to hundreds of nanometers. These nanostructures could self-assemble at room temperature in physiological buffers.

Science, this issue p. eaam5488; see also p. 1261

ARTICLE TOOLS

<http://science.sciencemag.org/content/355/6331/eaam5488>

SUPPLEMENTARY MATERIALS

<http://science.sciencemag.org/content/suppl/2017/03/22/355.6331.eaam5488.DC1>

RELATED CONTENT

<http://science.sciencemag.org/content/sci/355/6331/1261.full>

REFERENCES

This article cites 49 articles, 21 of which you can access for free
<http://science.sciencemag.org/content/355/6331/eaam5488#BIBL>

PERMISSIONS

<http://www.sciencemag.org/help/reprints-and-permissions>

Use of this article is subject to the [Terms of Service](#)